REPORT NO.
UCB/SESM-85/04

STRUCTURAL ENGINEERING AND
STRUCTURAL MECHANICS

A CONSISTENT RETURN MAPPING ALGORITHM FOR PLANE STRESS ELASTOPLASTICITY

by

JUAN C. SIMO

and

ROBERT L. TAYLOR

MAY 1985

DEPARTMENT OF CIVIL ENGINEERING
UNIVERSITY OF CALIFORNIA
BERKELEY, CALIFORNIA

A Return Mapping Algorithm for Plane Stress Elastoplasticity.

J.C. SIMO

Applied Mechanics Division,
Stanford University, Stanford, CA 94305.

and

R. L. TAYLOR

Structural Engineering and Structural Mechanics Division,
University of California, Berkeley, CA 94720.

Abstract

An unconditionally stable algorithm for *plane stress* elastoplasticity is developed, based upon the notion of elastic predictor return mapping (plastic corrector). Enforcement of the consistency condition is shown to reduce to the solution of a simple nonlinear equation. *Consistent* elastoplastic tangent moduli are obtained by *exact linearization* of the algorithm. Use of these moduli is essential in order to preserve the asymptotic rate of quadratic convergence of Newton methods. An exact solution for constant strain rate over the typical time step is derived. On the basis of this solution the accuracy of the algorithm is assessed by means of iso-error maps. The excellent performance of the algorithm for large time steps is illustrated in numerical experiments.

Contents

Introduction

The *radial return* algorithm initially proposed by Wilkins [1964], is the most widely used integration procedure for plane strain and three dimensional classical J_2 elastoplasticity. Extensions of this basic algorithm to account for isotropic and kinematic hardening have been developed by Krieg & Key [1976]. The procedure is now well established due mainly to the pionering accuracy analysis of Krieg & Krieg [1977] for ideal plasticity, subsequently extended by Schreyer, Kulak and Kramer [1979] to include hardening effects. Yoder & Whirley [1983] have demonstrated the overall superiority of the radial return method over other proposed algorithm, particularly in the presence of hardening.

The radial return algorithm is a particular case of elastic predictor-plastic corrector algorithms where a purely elastic *trial state* is followed by a plastic corrector phase (*return*

mapping). The purpose of the latter is to enforce consistency at the end of the step in a manner consistent with the prescribed flow rule. This notion has also been employed in non-classical plasticity models such as the *cap* model, Sandler & Rubin [1977]. The mathematical structure of this class of methods is now well understood in the context of linear kinematics, Ortiz [1981]. These integration procedures are simply *product formula* algorithms arising from an operator split on the elastoplastic problem of evolution. As emphasized by Moss [1984], return mapping algorithms always have been strain driven. Formulation of these notions in the finite deformation range are given in Simo and Ortiz [1985], and Simo [1985]. The stability of integration procedures for inelasticity is addressed in Argyris et. al. [1979], and recently, thoroughly re-examined in Ortiz & Popov [1985].

Three dimensional return mapping algorithms can be trivially modified for the *plane strain* problem (e.g. Hallquist [1983]). This is in contrast with the *plane stress* situation where satisfaction of the plane stress condition places a nontrivial constraint on the return algorithm. Hence, incremental methods based on the use of the classical elastoplastic moduli are still widely used, see, e.g., Marques [1984], Zienkiewicz , Sec **18.4** [1977] and references therein. On the computational side, iterative corrections to the radial return method have been proposed, Nagtegaal [1985], Hallquist et. al. [1985]. To some extent these procedures are developed on an *ad hoc* basis.

In this paper a family of return mapping algorithms for the plane stress problem is developed. The basic idea is to project the basic elastoplastic equations onto the subspace defined by the plane stress condition, and there construct a return algorithm by application of the generalized midpoint rule. Thus, the plane stress condition is identically satisfied by the algorithm. Exact (algorithmic) enforcement of the consistency condition is shown to yield a scalar equation for the plastic Lagrange parameter. For the case of isotropic elasticity the procedure takes a remarkably simple form due to the structure of the elastic matrix. For three dimensional elastoplasticity, use of the generalized midpoint rule was proposed by Rice and Tracy [1973], and subsequently extended by Ortiz and Popov [1985]. For viscoplasticity, it was employed by Hughes and Taylor [1978].

An essential ingredient in the overall performance of the algorithm is the development of consistent elastoplastic tangent moduli obtained by *linearization of the algorithm*. These moduli reduce to the classical elastoplastic moduli as the time step $h \to 0$ (consistency requirement). For finite values of h, however, use of the classical elastoplastic moduli results in loss of the asymptotic rate of quadratic convergence characteristic of Newton's methods, Simo & Taylor [1985]. We note that replacement of the classical elastoplastic moduli by the consistent moduli does not entail additional computational effort. It is also noted that enforcement of the consistency condition at $t_{n+\alpha}$ is essential in order to preserve the symmetry of the *consistent* elastoplastic moduli. It is shown that enforcement of consistency at the end of the step, as suggested by Ortiz & Popov [1985], results in *loss* of symmetry of algorithmic elastoplastic moduli.

Finally, the *exact* solution for the plane stress problem is obtained under the customary assumption of constant strain rate over the time step. This solution is compared with the proposed algorithm and used to develop isoerror maps.

The excellent performance of the proposed algorithm is illustrated by means of numerical simulations.

1. Formulation of the constrained equations.

In what follows *plane stress* elastoplasticity with nonlinear isotropic and linear kinematic hardening, and a von Mises yield condition is adopted as a model problem There is no conceptual difficulty in extending the ideas discussed below to other yield conditions, flow rule and hardening laws. Employing standard notation the *three dimensional* elastoplastic equations may be formulated in component form as

$$\begin{aligned} \epsilon_{ij} &= \epsilon^e_{ij} + \epsilon^p_{ij} \\ \dot{\epsilon}^p_{ij} &= \dot{\lambda}(s_{ij} - \alpha'_{ij}) \\ \dot{\alpha}'_{ij} &= \tfrac{2}{3} H \dot{\epsilon}^p_{ij} \\ \phi &\equiv \tfrac{1}{2} s_{ij} s_{ij} - \tfrac{1}{3}\kappa(\bar{e}^p) \le 0 \end{aligned} \tag{1.1a}$$

Here, s_{ij} are the components of the stress deviator defined as $s_{ij} := \sigma_{ij} - (\sigma_{kk}/3)\delta_{ij}$, where δ_{ij} is the Kronecker delta. Further, α'_{ij} are the components of the *back stress*, with $\alpha'_{kk} \equiv 0$. The function $\bar{e}^p \to \kappa(\bar{e}^p)$ defines the hardening law in terms of the the so-called *equivalent plastic strain* $\bar{e}^p$. The latter is defined by the rate equation

$$\dot{\bar{e}}^p = [\tfrac{2}{3}\dot{\epsilon}^p_{ij}\dot{\epsilon}^p_{ij}]^{1/2}, \tag{1.1b}$$

To equations (1.1a) and (1.1b) one has to append the elastic stress-strain relations

$$\sigma_{ij} = D_{ijkl}\epsilon^e_{kl} \tag{1.1c}$$

Constrained equations. The plane stress constraint may be systematically introduced as follows. Let V^S be the vector space of *symmetric* rank-2 stress tensors. Thus, *dim* $V^S = 6$. The *plane stress* subspace V^P is obtained from *three* constraints as

$$V^P := \{\ \boldsymbol{\sigma}\in V^S \quad | \quad \sigma_{13} \equiv \sigma_{23} = \sigma_{33} \equiv 0\ \} \tag{1.2a}$$

Similarly, the *deviator* subspace V^D is defined by *three* constraints

$$V^D := \{\ \mathbf{s}\in V^S \quad | \quad s_{13} \equiv s_{23} = 0, \text{ and } \sigma_{kk} \equiv 0\ \} \tag{1.2b}$$

Hence,*dim* V^P = *dim* V^D = 3. Since both V^D and V^P are isomorphic to $\mathbb{R}^3$ it proves convenient to introduce vector notation and express $\boldsymbol{\sigma}\in V^P$ and $\mathbf{s}\in V^D$ as

$$\boldsymbol{\sigma} := [\sigma_{11} \quad \sigma_{22} \quad \sigma_{12}]^t, \qquad \mathbf{s} := [s_{11} \quad s_{22} \quad s_{12}]^t \tag{1.3}$$

The mapping $\mathbf{P} : V^P \to V^D$ connecting the *constrained* stress tensor $\boldsymbol{\sigma}\in V^P$ and its deviator $\mathbf{s}\in V^D$ plays a crucial role in what follows. In matrix notation we have

$$\mathbf{s} \equiv \mathbf{P}\boldsymbol{\sigma}, \qquad \mathbf{P} := \tfrac{1}{3}\begin{bmatrix} 2 & -1 & 0 \\ -1 & 2 & 0 \\ 0 & 0 & 3 \end{bmatrix} \tag{1.4}$$

Note that the component s_{33} is *non zero* but is not explicitly included in (1.4). Instead of employing the three dimensional components α'_{ij} of the back stress directly, we introduce a vector $\boldsymbol{\alpha}\in V^P$ (i.e.,$\alpha'_{13} = \alpha'_{23} = \alpha'_{kk} = 0$) by the relation

$$[\alpha'_{11} \quad \alpha'_{11} \quad \alpha'_{12}]^t =: \mathbf{P}\boldsymbol{\alpha}, \qquad \boldsymbol{\alpha} := [\alpha_{11} \quad \alpha_{22} \quad \alpha_{12}]^t. \tag{1.5}$$

Finally, the components of the strain tensors are collected in vector form as

$$\boldsymbol{\epsilon} := [\epsilon_{11} \quad \epsilon_{22} \quad 2\epsilon_{12}]^t, \qquad \boldsymbol{\epsilon}^p := [\epsilon^p_{11} \quad \epsilon^p_{22} \quad 2\epsilon^p_{12}]^t \tag{1.6}$$

With this notation at hand, the basic equations (1.1) may be reformulated in vector form as follows

$$\begin{aligned} \boldsymbol{\epsilon} &= \boldsymbol{\epsilon}^e + \boldsymbol{\epsilon}^p \\ \boldsymbol{\sigma} &= \mathbf{D}\boldsymbol{\epsilon}^e \\ \dot{\boldsymbol{\epsilon}}^p &= \dot{\lambda}\mathbf{P}\boldsymbol{\eta} \\ \dot{\boldsymbol{\alpha}} &= \dot{\lambda}H\boldsymbol{\eta} \\ \phi &:= \tfrac{1}{2}\boldsymbol{\eta}^t\mathbf{P}\boldsymbol{\eta} - \tfrac{1}{3}\kappa^2(\bar{e}^p) \le 0 \end{aligned} \tag{1.7}$$

where $\mathbf{D}$ is the elastic constitutive matrix for plane stress, and we have set for convenience

$$\boldsymbol{\eta} := \boldsymbol{\sigma} - \boldsymbol{\alpha} \tag{1.8}$$

Further, by making use of the flow rule $(1.7)_3$ and relation (1.4) for the stress deviator, the rate equation (1.1b) may be recast as

$$\dot{\bar{e}}^p = [\tfrac{2}{3}\boldsymbol{\eta}^t \mathbf{P}\boldsymbol{\eta}]^{1/2}\dot{\lambda} \tag{1.9}$$

Finally, loading/unloading conditions may be conveniently formulated in standard Kuhn-Tucker form simply by requiring that

$$\phi \le 0, \quad \dot{\lambda} \ge 0, \quad \dot{\lambda}\phi \equiv 0 \tag{1.10}$$

Note that conditions (1.10) are consistent with the classical notion of loading/unloading. As an illustration, if $\phi < 0$ then $(1.10)_3$ requires that $\dot{\lambda} \equiv 0$; hence $\dot{\boldsymbol{\epsilon}}^p \equiv \mathbf{0}$ and $\dot{\bar{e}}^p \equiv 0$ so that the process is elastic.

Remark 1.1. For the case of *isotropic* elasticity the constitutive matrix $\mathbf{D}$ and $\mathbf{P}$ have the same characteristic subspaces; i.e., their spectral decomposition is given by

$$\mathbf{P} = \mathbf{Q}\mathbb{A}_{\mathbf{P}}\mathbf{Q}^t, \qquad \mathbf{D} = \mathbf{Q}\mathbb{A}_{\mathbf{D}}\mathbf{Q}^t, \tag{1.11a}$$

where the orthogonal matrix $\mathbf{Q} \equiv \mathbf{Q}^t$ and the constitutive matrix $\mathbf{D}$ are given by

$$\mathbf{Q} = \frac{1}{\sqrt{2}}\begin{bmatrix} 1 & -1 & 0 \\ 1 & 1 & 0 \\ 0 & 0 & \sqrt{2} \end{bmatrix}, \qquad \mathbf{D} := \frac{E}{1-\nu^2}\begin{bmatrix} 1 & \nu & 0 \\ \nu & 1 & 0 \\ 0 & 0 & \dfrac{1-\nu}{2} \end{bmatrix}. \tag{1.11b}$$

The diagonal matrices $\mathbb{A}_{\mathbf{P}}$ and $\mathbb{A}_{\mathbf{D}}$ have the expressions

$$\mathbb{A}_{\mathbf{P}} = \begin{bmatrix} \frac{1}{3} & 0 & 0 \\ 0 & 1 & 0 \\ 0 & 0 & 2 \end{bmatrix}, \quad \mathbb{A}_{\mathbf{D}} = \begin{bmatrix} \dfrac{E}{1-\nu} & 0 & 0 \\ 0 & 2G & 0 \\ 0 & 0 & G \end{bmatrix}. \tag{1.11c}$$

Since $\mathbf{P}$ and $\mathbf{D}$ have the same eigenvectors, it follows that $\mathbf{P}\mathbf{D} \equiv \mathbf{D}\mathbf{P}$; that is, $\mathbf{P}$ and $\mathbf{D}$ commute. For isotropic elasticity, the properties recorded above play a crucial role in the implementation of the algorithm discussed in Section 3. □

Remark 1.2. It should be noted that the strain components ϵ_{33}, ϵ^e_{33}, and ϵ^p_{33} do not enter the formulation explicitly. These are *dependent* variables obtained from the basic variables $\{\boldsymbol{\epsilon}, \boldsymbol{\epsilon}^p, \boldsymbol{\sigma}\}$, the plane stress condition, and the condition of isochoric plastic flow. For the case of isotropic elasticity we have

$$\epsilon^e_{33} = -\nu(\epsilon^e_{11} + \epsilon^e_{22}), \qquad \epsilon^p_{33} = -\epsilon^p_{11} - \epsilon^p_{22} \tag{1.12}$$

The total strain ϵ_{33} then follows simply as $\epsilon_{33} \equiv \epsilon^e_{33} + \epsilon^p_{33}$ □

We conclude this section by recording the expression for the so-called *elastoplastic tangent moduli*. Although the argument is fairly standard (e.g., Owen & Hinton [1980, page 227]) for comparison purposes with our developments in Section 2.3 we outline the main steps. By time differentiation of equation $(1.7)_2$ it follows that

$$\dot{\boldsymbol{\sigma}} = \mathbf{D}(\dot{\boldsymbol{\epsilon}} - \dot{\lambda}\mathbf{P}\boldsymbol{\eta}) \tag{1.13}$$

For plastic loading, the *plastic consistency* condition requires that the stress point must remain on the yield surface. Accordingly, $\phi = 0$ and $\dot{\phi} \equiv 0$. This latter condition implies

$$\dot{\phi} = \boldsymbol{\eta}^t \mathbf{P}\dot{\boldsymbol{\eta}} - \tfrac{2}{3}\kappa\kappa'\dot{\bar{e}}^p \equiv 0 \tag{1.14}$$

where $\kappa' := \partial\kappa/\partial\bar{e}^p$. Substitution of $(1.7)_4$, (1.8) and (1.13) into (1.14) yields

$$\dot{\lambda} = \frac{\boldsymbol{\eta}^t \mathbf{P}\mathbf{D}\dot{\boldsymbol{\epsilon}}}{\boldsymbol{\eta}^t \mathbf{P}\mathbf{D}\mathbf{P}\boldsymbol{\eta}(1+\beta)} \tag{1.15}$$

where we have set

$$\beta := \frac{2}{3}\frac{(\kappa' + H)\bar{\phi}^2}{\boldsymbol{\eta}^t \mathbf{P}\mathbf{D}\mathbf{P}\boldsymbol{\eta}}, \qquad \bar{\phi} := \sqrt{\boldsymbol{\eta}^t \mathbf{P}\boldsymbol{\eta}} \tag{1.16}$$

Finally, substitution of (1.15) into (1.13) leads to the expression

$$\frac{d\boldsymbol{\sigma}}{d\boldsymbol{\epsilon}} = \mathbf{D} - \frac{\mathbf{n}\otimes\mathbf{n}}{1+\beta}, \qquad \mathbf{n} := \frac{\mathbf{D}\mathbf{P}\boldsymbol{\eta}}{\sqrt{\boldsymbol{\eta}^t \mathbf{P}\mathbf{D}\mathbf{P}\boldsymbol{\eta}}} \tag{1.17}$$

where the symbol "$\otimes$" denotes tensor product (i.e., in matrix notation $\mathbf{n}\otimes\mathbf{n} \rightarrow \mathbf{n}\mathbf{n}^t$). □

2. Integration algorithm.

In this section we develop the integration procedure for constitutive equations (1.7). From a computational standpoint it is essential to note that this problem of evolution may always be regarded as *strain* driven in the following sense.

2.1. Basic problem. Let $[0, T]\subset\mathbb{R}$ be the time interval of interest. At time $t_n\in[0, T]$ we assume that the total and plastic strain fields and the back stress are known; that is

$$\{\boldsymbol{\epsilon}_n, \boldsymbol{\epsilon}_n^p, \bar{e}^p, \boldsymbol{\alpha}_n\} \quad \text{given data at} \quad t_n \tag{2.1}$$

It is noted that the *elastic strain* tensor and the *stress* tensor are regarded as *dependent* variables which can always be obtained from the basic variables (2.1) through the relations

$$\boldsymbol{\epsilon}_n^e \equiv \boldsymbol{\epsilon}_n - \boldsymbol{\epsilon}_n^p, \qquad \boldsymbol{\sigma}_n = \mathbf{D}\boldsymbol{\epsilon}_n^e. \tag{2.2}$$

Let $\mathbf{u}:\Omega\rightarrow\mathbb{R}^3$ be the incremental displacement field *assumed to be given*. Here, $\Omega\subset\mathbb{R}^3$ is the reference configuration of the body of interest. The basic problem, then, is to update the fields (2.1) to $t_{n+1}\in[0, T]$ in a manner consistent with the elastoplastic constitutive equations (1.7). Note that the stress field $\boldsymbol{\sigma}_{n+1}$ is computed from (2.2) once the strain field is known. The problem is strain driven in the sense that the total strain tensor $\boldsymbol{\epsilon}$ is trivially updated according to the (exact) formula

$$\boldsymbol{\epsilon}_{n+1} = \boldsymbol{\epsilon}_n + \nabla^S \mathbf{u} \tag{2.3}$$

where $\nabla^S(\,\cdot\,)$ denotes the symmetric gradient, and $\mathbf{u}$ is the specified displacement increment over the time step $[t_n, t_{n+1}]$. It remains to update the plastic strain tensor $\boldsymbol{\epsilon}^p$ and the equivalent plastic strain $\bar{e}^p$.

2.2. Integration algorithm. The plastic strains $\boldsymbol{\epsilon}_{n+1}^p$ and $\bar{e}_{n+1}^p$, and the back stress $\boldsymbol{\alpha}_{n+1}$, are determined by integration of the flow rule and hardening law over the time step $[t_n, t_{n+1}]\subset[0, T]$. To this end, use is made of the *generalized midpoint rule*. Introducing the notation

$$\boldsymbol{\epsilon}_{n+\alpha} := \alpha\boldsymbol{\epsilon}_{n+1} + (1-\alpha)\boldsymbol{\epsilon}_n \equiv \boldsymbol{\epsilon}_n + \alpha\nabla^S\mathbf{u}, \qquad \alpha\in[0, 1] \tag{2.4}$$

the integration algorithm may be formulated as †

$$\begin{aligned}
\boldsymbol{\epsilon}_{n+1}^p &= \boldsymbol{\epsilon}_n^p + \lambda\mathbf{P}\boldsymbol{\eta}_{n+\alpha} \\
\bar{e}_{n+1}^p &= \bar{e}_n^p + \lambda\sqrt{\tfrac{2}{3}}\bar{\phi}_{n+\alpha} \\
\boldsymbol{\alpha}_{n+1} &= \boldsymbol{\alpha}_n + \tfrac{2}{3}H\boldsymbol{\eta}_{n+\alpha}
\end{aligned} \tag{2.5}$$

† In the following, for notational simplicity, $\Delta\lambda$ is replaced by λ.

where $\boldsymbol{\eta}_{n+\alpha}$ and $\bar{\phi}_{n+\alpha}$ are defined as follows. First, $\boldsymbol{\alpha}_{n+\alpha}$, $\boldsymbol{\epsilon}^p_{n+\alpha}$, and $\boldsymbol{\sigma}_{n+\alpha}$ are defined according to the expressions

$$\begin{aligned} \boldsymbol{\epsilon}^p_{n+\alpha} &:= \alpha\,\boldsymbol{\epsilon}^p_{n+1} + (1-\alpha)\,\boldsymbol{\epsilon}^p_n \\ \boldsymbol{\alpha}_{n+\alpha} &:= \alpha\,\boldsymbol{\alpha}_{n+1} + (1-\alpha)\,\boldsymbol{\alpha}_n \\ \boldsymbol{\sigma}_{n+\alpha} &:= \mathbf{D}[\boldsymbol{\epsilon}_{n+\alpha} - \boldsymbol{\epsilon}^p_{n+\alpha}] \end{aligned} \tag{2.6}$$

Then $\boldsymbol{\eta}_{n+\alpha}$ and $\bar{\phi}_{n+\alpha}$ are obtained through the expressions

$$\boldsymbol{\eta}_{n+\alpha} := \boldsymbol{\sigma}_{n+\alpha} - \boldsymbol{\alpha}_{n+\alpha}, \qquad \bar{\phi}_{n+\alpha} := \sqrt{\boldsymbol{\eta}^t_{n+\alpha}\mathbf{P}\,\boldsymbol{\eta}_{n+\alpha}}. \tag{2.7}$$

Note that $(2.6)_3$ is simply the stress strain relation $(1.7)_2$ at $t_{n+\alpha}$, with the additive decomposition $(1.7)_1$ implicitly used. The basic update algorithm (2.5) may be recast in terms of $\boldsymbol{\sigma}_{n+\alpha}$ by making use of (2.6) and (2.7). This leads to the following sequential update procedure

$$\begin{aligned} \boldsymbol{\epsilon}_{n+\alpha} &= \boldsymbol{\epsilon}_n + \alpha\nabla^S \mathbf{u} \\ \boldsymbol{\eta}_{n+\alpha} &= \frac{1}{1+\frac{2}{3}\alpha\lambda H}\,\mathbb{Z}(\lambda)[\boldsymbol{\epsilon}_{n+\alpha} - \boldsymbol{\epsilon}^p_n - \mathbf{D}^{-1}\boldsymbol{\alpha}_n] \\ \boldsymbol{\alpha}_{n+1} &= \boldsymbol{\alpha}_n + \alpha\lambda H\,\boldsymbol{\eta}_{n+\alpha} \\ \boldsymbol{\sigma}_{n+\alpha} &= \boldsymbol{\eta}_{n+\alpha} - \boldsymbol{\alpha}_{n+\alpha} \\ \bar{e}^p_{n+\alpha} &= \bar{e}^p_n + \alpha\sqrt{\tfrac{2}{3}}\,\lambda\,\bar{\phi}_{n+\alpha} \end{aligned} \tag{2.8}$$

Here, $\mathbb{Z}(\lambda)$ plays the role of a modified (*algorithmic*) elastic tangent matrix and is defined as

$$\mathbb{Z}(\lambda) := [\mathbf{D}^{-1} + \frac{\alpha\lambda}{1+\alpha\frac{2}{3}H\lambda}\mathbf{P}]^{-1} \tag{2.9}$$

The update formulae (2.8) depend parametrically on the plastic Lagrange multiplier λ which is to be determined by enforcing the condition that the stress point $\boldsymbol{\sigma}_{n+\alpha}$ *at time* $t_{n+\alpha}$ is on the yield surface. That is, by enforcing *consistency at* $t_{n+\alpha}$. Accordingly, we have the constraint condition

$$\phi_{n+\alpha}(\lambda) := \tfrac{1}{2}\,\boldsymbol{\eta}^t_{n+\alpha}\mathbf{P}\,\boldsymbol{\eta}_{n+\alpha} - \tfrac{1}{3}\kappa^2(\bar{e}^p_{n+\alpha}) \equiv 0 \tag{2.10}$$

This furnishes a nonlinear scalar equation which may be solved for λ. For the case of isotropic elasticity condition (2.10) has a particularly simple form due to the structure of matrices $\mathbf{P}$ and $\mathbf{D}$, and may be easily solved by elementary methods, as shown in Section 3. □

Remark 2.1. It is again emphasized that the algorithmic counterpart of the consistency condition is enforced at the mid-step $t_{n+\alpha}$, and *not at* the end of the step t_{n+1}. It is shown below that enforcement of the consistency condition at t_{n+1}, as in Ortiz & Popov [1985], leads to *consistent* elastoplastic moduli which are *non-symmetric*. □

Remark 2.2. The algorithm (2.8) (or (2.5)) depends on the time step $h := t_{n+1} - t_n$. By expanding the exact solution $\{\boldsymbol{\epsilon}^p(t_n+h), \bar{e}^p(t_n+h), \boldsymbol{\alpha}(t_n+h)\}$ at time t_{n+1} in a Taylor series about t_n and using (1.7), it can be readily shown that (2.5) is *second order accurate* for $\alpha = \frac{1}{2}$, as expected, and first order accurate otherwise. For an explicit calculation of this type we refer to Ortiz & Popov [1985]. □

2.3. Consistent elastoplastic tangent moduli.

We develop elastoplastic tangent moduli by linearization of the algorithm (2.8). It is shown that the resulting tangent operator reduces in the limit as the step size $h \to 0$ to the classical elastoplastic moduli defined by (1.17). This is essentially the consistency requirement between algorithm (2.8) and problem (1.7). However, as shown in Simo & Taylor [1985], for finite values of h it is essential to use the consistent tangent moduli in order to preserve the quadratic rate of asymptotic convergence that characterizes Newton's method.

By differentiation of the algorithm we obtain the following formulae

$$\begin{aligned} d\boldsymbol{\sigma}_{n+\alpha} &= \mathbf{D}[d\boldsymbol{\epsilon}_{n+\alpha} - d\lambda\,\alpha\,\mathbf{P}\boldsymbol{\eta}_{n+\alpha} - \lambda\,\alpha\,\mathbf{P}(d\boldsymbol{\sigma}_{n+\alpha} - d\boldsymbol{\alpha}_{n+\alpha})] \\ d\bar{e}^{p}_{n+\alpha} &= \sqrt{\tfrac{2}{3}}\,\alpha[\bar{\phi}_{n+\alpha}\,d\lambda + \lambda\,d\bar{\phi}_{n+\alpha}] \\ d\boldsymbol{\alpha}_{n+\alpha} &= \frac{\frac{2}{3}\alpha H}{1+\frac{2}{3}\alpha\lambda H'}[d\lambda\,\boldsymbol{\eta}_{n+\alpha} + \lambda\,d\boldsymbol{\sigma}_{n+\alpha}] \end{aligned} \tag{2.11}$$

where $\bar{\phi}_{n+\alpha}$ is defined by $(2.7)_2$ and $d\bar{\phi}_{n+\alpha}$ is computed by differentiating this expression. From $(2.11)_1$ and $(2.11)_3$ it follows that

$$d\boldsymbol{\sigma}_{n+\alpha} = \mathbb{Z}(\lambda)\Big[d\boldsymbol{\epsilon}_{n+\alpha} - \frac{\alpha\,d\lambda}{1+\frac{2}{3}\alpha\lambda H}\mathbf{P}\boldsymbol{\eta}_{n+\alpha}\Big] \tag{2.12}$$

Differentiation of the consistency condition (2.10) at $t_{n+\alpha}$ and use of $(2.11)_2$ leads to

$$d\phi_{n+\alpha} \equiv (1-\alpha\tfrac{2}{3}\kappa'_{n+\alpha})\bar{\phi}_{n+\alpha}\,d\bar{\phi}_{n+\alpha} - \tfrac{2}{3}\alpha\kappa'_{n+\alpha}\bar{\phi}^{2}_{n+\alpha}\,d\lambda \equiv 0 \tag{2.13}$$

By making use of $(2.11)_3$, (2.12), (2.13) and solving for $d\lambda$, the following expression is obtained

$$\frac{\alpha\,d\lambda}{\gamma_1} = \frac{\boldsymbol{\eta}^{t}_{n+\alpha}\mathbf{P}\mathbb{Z}\,d\boldsymbol{\epsilon}_{n+\alpha}}{\boldsymbol{\eta}^{t}_{n+\alpha}\mathbf{P}\mathbb{Z}\mathbf{P}\boldsymbol{\eta}_{n+\alpha}(1+\beta_{n+\alpha})}, \qquad \gamma_1 := 1+\tfrac{2}{3}\alpha H\lambda \tag{2.14a}$$

where

$$\beta_{n+\alpha} := \frac{\frac{2}{3}\bar{\phi}^{2}_{n+\alpha}(\kappa'_{n+\alpha}\gamma_1 + H\gamma_2)\gamma_1}{\boldsymbol{\eta}^{t}_{n+\alpha}\mathbf{P}\mathbb{Z}\mathbf{P}\boldsymbol{\eta}_{n+\alpha}\gamma_2}, \qquad \gamma_2 := 1-\tfrac{2}{3}\alpha\kappa'_{n+\alpha}\lambda \tag{2.14b}$$

From (2.14) and (2.12) we finally obtain

$$\left.\frac{d\boldsymbol{\sigma}}{d\boldsymbol{\epsilon}}\right|_{n+\alpha} = \mathbb{Z} - \frac{\mathbf{N}_{n+\alpha}\otimes\mathbf{N}_{n+\alpha}}{1+\beta_{n+\alpha}} \tag{2.15a}$$

where we have set

$$\mathbf{N}_{n+\alpha} := \frac{\mathbb{Z}\mathbf{P}\boldsymbol{\eta}_{n+\alpha}}{\sqrt{\boldsymbol{\eta}^{t}_{n+\alpha}\mathbf{P}\mathbb{Z}\mathbf{P}\boldsymbol{\eta}_{n+\alpha}}} \tag{2.15b}$$

The elastoplastic tangent moduli at t_{n+1} now follow at once from (2.14) by a chain rule argument. One simply finds that

$$\left.\frac{d\boldsymbol{\sigma}}{d\boldsymbol{\epsilon}}\right|_{n+1} = \frac{d\boldsymbol{\sigma}_{n+1}}{d\boldsymbol{\sigma}_{n+\alpha}} : \left.\frac{d\boldsymbol{\sigma}}{d\boldsymbol{\epsilon}}\right|_{n+\alpha} : \frac{d\boldsymbol{\epsilon}_{n+\alpha}}{d\boldsymbol{\epsilon}_{n+1}} \equiv \left.\frac{d\boldsymbol{\sigma}}{d\boldsymbol{\epsilon}}\right|_{n+\alpha} \tag{2.16}$$

Remark 2.3. It is noted that as the time step $h \to 0$ one has $\lambda \to 0$. From expressions $(2.14)_2$ it follows that $\gamma_1 \to 1$ and $\gamma_2 \to 1$ as $h \to 0$. Hence

$$h \to 0 \quad \Rightarrow \quad \mathbb{Z}(\lambda) \to \mathbf{D} \quad \text{and} \quad \beta_{n+\alpha} \to \beta, \tag{2.17}$$

where β is given by (1.16). Therefore, the "consistent" elastoplastic moduli (2.14) reduce to the classical elastoplastic moduli given by (1.17) as $h \to 0$. This shows that algorithm (2.4) is *consistent* with problem (1.7). □

Remark 2.4. We examine the implication of enforcing the plastic consistency condition at t_{n+1}. For the sake of simplicity in the exposition the case of perfect plasticity ($R \equiv$ constant, and $H \equiv 0$) is considered. If the stress point is required to be on the yield surface at t_{n+1}, then instead of condition (2.10) one has

$$\phi_{n+1}(\lambda) \equiv \tfrac{1}{2}\boldsymbol{\sigma}_{n+1}^t \mathbf{P}\boldsymbol{\sigma}_{n+1} - R^2 \equiv 0 \tag{2.18}$$

To determine the value of $d\lambda$ we note that

$$d\boldsymbol{\sigma}_{n+1} = \mathbf{D}\, d\boldsymbol{\epsilon}_{n+1} = \frac{1}{\alpha}\mathbf{D}\, d\boldsymbol{\epsilon}_{n+\alpha} = \frac{1}{\alpha} d\boldsymbol{\sigma}_{n+\alpha}, \qquad \alpha > 0 \tag{2.19}$$

By differentiating $(2.18)_1$ and making use of (2.19) along with (2.12) we obtain the expression

$$\alpha\, d\lambda = \frac{\boldsymbol{\sigma}_{n+1}^t \mathbf{P}\boldsymbol{\mathcal{E}}\, d\boldsymbol{\epsilon}_{n+\alpha}}{\boldsymbol{\sigma}_{n+1}^t \mathbf{P}\boldsymbol{\mathcal{E}}\mathbf{P}\boldsymbol{\sigma}_{n+\alpha}} \tag{2.20}$$

Substitution of (2.20) into (2.12) leads to

$$\left.\frac{d\boldsymbol{\sigma}}{d\boldsymbol{\epsilon}}\right|_{n+1} = \boldsymbol{\mathcal{E}} - \frac{[\boldsymbol{\mathcal{E}}\mathbf{P}\boldsymbol{\sigma}_{n+1}] \otimes [\boldsymbol{\mathcal{E}}\mathbf{P}\boldsymbol{\sigma}_{n+\alpha}]}{\boldsymbol{\sigma}_{n+1}^t \mathbf{P}\boldsymbol{\mathcal{E}}\mathbf{P}\boldsymbol{\sigma}_{n+\alpha}} \tag{2.21}$$

Clearly, expression (2.21) is *non-symmetric* except for the special case of $\alpha = 1$. Thus, for the generalized mid-point rule algorithm, the consistency condition must be enforced at the mid-step $t_{n+\alpha}$. Otherwise, the resulting *consistent* elastoplastic moduli are *non-symmetric*. □

Remark 2.5. The stability requirement of algorithm (2.8) is the one typically found for the generalized midpoint rule; i.e., *unconditional stability* is attained for $\alpha \geq \tfrac{1}{2}$. This result is classical for linear elastodynamics, see e.g. the review article of Hughes [1983]. In the context of viscoplasticity, a similar result was found by Hughes & Taylor [1978]. For elastoplasticity, the sharp stability analysis of Ortiz & Popov [1985] again confirms the same result. □

Remark 2.6 The basic algorithm (2.4)-(2.5) may be viewed as a *product formula* arising from the following *operator split* on the elastoplastic problem of evolution.

Total	≡	*Elastic Predictor*	+	*Plastic Corrector*
$\dot{\boldsymbol{\epsilon}} = given$		$\dot{\boldsymbol{\epsilon}} = given$		$\dot{\boldsymbol{\epsilon}} = 0$
$\dot{\boldsymbol{\epsilon}}^p = \dot{\lambda}\mathbf{P}\boldsymbol{\eta}$		$\dot{\boldsymbol{\epsilon}}^p = 0$		$\dot{\boldsymbol{\epsilon}}^p = \dot{\lambda}\mathbf{P}\boldsymbol{\eta}$
$\dot{\bar{e}}^p = \dot{\lambda}[\frac{2}{3}\boldsymbol{\eta}^t \mathbf{P}\boldsymbol{\eta}]^{1/2}$		$\dot{\bar{e}}^p = 0$		$\dot{\bar{e}}^p = \dot{\lambda}[\frac{2}{3}\boldsymbol{\eta}^t \mathbf{P}\boldsymbol{\eta}]^{1/2}$
$\dot{\boldsymbol{\alpha}} = \dot{\lambda}\frac{2}{3}H\boldsymbol{\eta}$		$\dot{\boldsymbol{\alpha}} = \mathbf{0}$		$\dot{\boldsymbol{\alpha}} = \dot{\lambda}\frac{2}{3}H\boldsymbol{\eta}$

The geometric update formula (2.4) defines an (exact) algorithm consistent with the elastic predictor problem. Note that the elastic relations $(1.7)_2$ are regarded as a constraint that hold at all time. By computing the stress tensor at the elastic predictor phase one obtains the so-called trial elastic stress. The second part of the algorithm defines a relaxation process towards the yield surface often referred as *return mapping*. Operator splits and product formulae have long tradition in the computational literature, see e.g., Chorin et. al [1978]. For elastoplasticity, the radial return method proposed by Wilkins [1960] furnishes the best known example. A thorough analysis is contained in Krieg & Krieg [1977], and subsequently extended by Schreyer, Kulak & Kramer [1979]. □

3. Implementation.

For the case of isotropic elasticity, the implementation of the algorithm discussed above takes a remarkably simple form. Employing the same notation as in Remark 1.1 we define

$$\boldsymbol{\xi} := \mathbf{Q}^t\boldsymbol{\eta} \equiv [\frac{\eta_{11} - \eta_{22}}{\sqrt{2}} \quad \frac{\eta_{11} + \eta_{22}}{\sqrt{2}} \quad \eta_{12}]^t \tag{3.1}$$

where $\mathbf{Q}$ is given by $(1.11b)_1$. In addition, we define an *elastic trial* state given by $\boldsymbol{\sigma}_{n+\alpha}^E$, $\boldsymbol{\eta}_{n+\alpha}^E$ and $\boldsymbol{\xi}_{n+\alpha}^E$, by setting

$$\boldsymbol{\sigma}^E_{n+\alpha} := \mathbf{D}[\boldsymbol{\epsilon}_{n+1} - \boldsymbol{\epsilon}^p_n], \qquad \boldsymbol{\eta}^E_{n+\alpha} := \boldsymbol{\sigma}^E_{n+\alpha} - \boldsymbol{\alpha}_n, \qquad \boldsymbol{\xi}^E_{n+\alpha} := \mathbf{Q}^t\,\boldsymbol{\eta}^E_{n+\alpha} \tag{3.2}$$

Making use of relations (1.11) the basic update formula $(2.8)_2$ takes the form

$$\boldsymbol{\xi}_{n+1} = [(1+\alpha\tfrac{2}{3}\lambda H)\mathbf{I} + \alpha\lambda\,\mathbb{A}_P\,\mathbb{A}_D]^{-1}\,\boldsymbol{\xi}^E_{n+\alpha} \equiv \boldsymbol{\Gamma}(\lambda)\,\boldsymbol{\xi}^E_{n+\alpha} \tag{3.3}$$

where $\boldsymbol{\Gamma}(\lambda)$ is a diagonal matrix given by

$$\boldsymbol{\Gamma}(\lambda) := diag\left[\frac{1}{1+(\dfrac{E}{3(1-\nu)}+\frac{2}{3}H)\alpha\lambda}, \frac{1}{1+\alpha(2G+\frac{2}{3}H)\lambda}, \frac{1}{1+\alpha(2G+\frac{2}{3}H)\lambda}\right] \tag{3.4}$$

In terms of the $\boldsymbol{\xi}$ variables, the consistency condition (2.10) takes a simple form. For convenience, we set

$$\bar{\phi}^2(\lambda) := \frac{(\xi^E_{11})^2}{[1+(\dfrac{E}{3(1-\nu)}+\frac{2}{3}H)\alpha\lambda]^2} + \frac{(\xi^E_{22})^2+(\xi^E_{12})^2}{[1+\alpha(2G+\frac{2}{3}H)\lambda]^2}$$
$$R^2(\lambda) := \tfrac{1}{3}\kappa^2(\bar{e}^p + \alpha\sqrt{\tfrac{2}{3}}\,\bar{\phi}(\lambda)) \tag{3.5}$$

where $R(\lambda)$ is the radius of the yield surface defined in terms of the hardening rule (1.9). With this notation at hand equation (2.10) now reads

$$\phi(\lambda) = \tfrac{1}{2}\bar{\phi}^2(\lambda) - R^2(\lambda), \qquad \lambda \geq 0 \tag{3.6}$$

It can be readily shown that the function $\bar{\phi}^2(\lambda)$ is *monotonically* decreasing for $\lambda\in[0, \infty)$, and further that

$$\lim_{\lambda\to\infty}\bar{\phi}^2(\lambda) \equiv \lim_{\lambda\to\infty}\frac{d}{d\lambda}\bar{\phi}^2(\lambda) = 0 \tag{3.7}$$

Thus, for the physically meaningful case of a monotonically increasing hardening law, (3.6) has a *unique* solution $\lambda \geq 0$. In particular, linear and saturation laws of the exponential type are often used; i.e.,

$$\kappa(\bar{e}^p) = K\,\bar{e}^p + \kappa_0 + (\kappa_\infty - \kappa_0)[1 - \exp(-\gamma\,\bar{e}^p)] \tag{3.8}$$

Here, $K > 0$, $\kappa_\infty > \kappa_0$ and $\gamma > 0$ are material constants. □

Remark 3.1. Equation (3.6) is ideally suited for a local iterative solution procedure employing Newton's method. Note that in most realistic applications for which the hardening law is nonlinear, such as (3.8), a local iterative solution is always necessary, even for plane strain with von Mises yield condition (e.g. see Simo & Taylor [1985]). Thus, the additional effort required to solve (3.6) due to the presence of $\bar{\phi}^2(\lambda)$ is negligible. □

A step by step implementation of the algorithm discussed above is summarized for convenience in Box 1.

4. Numerical Examples

In this section attention is first focused on an assessment of the accuracy of the proposed algorithm by numerical testing. For this purpose, isoerror maps are developed on the basis of a strain controlled homogeneous problem. Subsequently, the robustness and overall performance of the solution procedure is illustrated by means of two numerical examples. All the calculation reported herein were performed in a VAX 11/750 under the Berkeley UNIX operating system.

BOX 1. *Algorithm for plane stress* ($\alpha = 1$)

- Update strain tensor. Compute trial elastic stresses

$$\epsilon_{n+1} = \epsilon_n + \nabla^S \mathbf{u}$$
$$\boldsymbol{\sigma}^E = \mathbf{D}[\epsilon_{n+1} - \epsilon_n^p]$$
$$\boldsymbol{\eta}^E = \boldsymbol{\sigma}^E - \boldsymbol{\alpha}_n$$

- Consistency at t_{n+1}: Solve $\phi(\lambda) = 0$ for λ

$$\phi(\lambda) := \tfrac{1}{2}\bar{\phi}^2(\lambda) - R^2(\lambda) \equiv 0$$

$$\bar{\phi}^2(\lambda) := \tfrac{1}{2}\frac{(\eta_{11}^E - \eta_{22}^E)^2}{[1 + (\frac{E}{3(1-\nu)} + \frac{2}{3}H)\lambda]^2} + \tfrac{1}{2}\frac{(\eta_{11}^E + \eta_{22}^E)^2 + (2\eta_{12}^E)^2}{[1 + (2G + \frac{2}{3}H)\lambda]^2}$$

$$R^2(\lambda) := \tfrac{1}{3}\kappa^2(\bar{e}_n^p + \alpha\sqrt{\tfrac{2}{3}}\bar{\phi}(\lambda))$$

- Compute modified (*algorithmic*) elastic tangent moduli

$$\boldsymbol{\Xi} := [\mathbf{D}^{-1} + \frac{\lambda}{1 + \frac{2}{3}\lambda H}\mathbf{P}]^{-1}$$

- Update stresses and plastic strains at t_{n+1}

$$\boldsymbol{\eta}_{n+1} = \frac{1}{1 + \frac{2}{3}\lambda H}\boldsymbol{\Xi}(\lambda)\mathbf{D}^{-1}\boldsymbol{\eta}^E$$

$$\boldsymbol{\alpha}_{n+1} = \boldsymbol{\alpha}_n + \lambda\tfrac{2}{3}H\boldsymbol{\eta}_{n+1}$$

$$\boldsymbol{\sigma}_{n+1} = \boldsymbol{\eta}_{n+1} - \boldsymbol{\alpha}_{n+1}$$
$$\bar{e}_{n+\alpha}^p = \bar{e}_n^p + \sqrt{\tfrac{2}{3}}\lambda\bar{\phi}(\lambda)$$
$$\epsilon_{n+1}^p = \epsilon_n^p + \lambda\mathbf{P}\boldsymbol{\eta}_{n+1}$$

- Compute *consistent* elastoplastic tangent moduli

$$\left.\frac{d\boldsymbol{\sigma}}{d\epsilon}\right|_{n+1} = \boldsymbol{\Xi} - \frac{[\boldsymbol{\Xi}\mathbf{P}\boldsymbol{\eta}_{n+1}][\boldsymbol{\Xi}\mathbf{P}\boldsymbol{\eta}_{n+1}]^t}{\boldsymbol{\eta}_{n+1}^t\mathbf{P}\boldsymbol{\Xi}\mathbf{P}\boldsymbol{\eta}_{n+1} + \bar{\beta}_{n+1}}$$

$$\gamma_1 := 1 + \tfrac{2}{3}H\lambda, \quad \gamma_2 := 1 - \tfrac{2}{3}\kappa'_{n+1}\lambda$$

$$\bar{\beta}_{n+1} := \tfrac{2}{3}\frac{\gamma_1}{\gamma_2}(\kappa'_{n+1}\gamma_1 + H\gamma_2)\boldsymbol{\eta}_{n+1}^t\mathbf{P}\boldsymbol{\eta}_{n+1}$$

- Update ϵ_{33} strain

$$\epsilon_{33n+1} = -\frac{\nu}{E}(\sigma_{11_{n+1}} + \sigma_{22_{n+1}}) - (\epsilon_{11_{n+1}}^p + \epsilon_{22_{n+1}}^p)$$

4.1 Accuracy analysis. Iso-error maps.

Isoerror maps corresponding to specified loading increments provide a systematic approach to test the accuracy of algorithms for elasto-plasticity. The procedure has been employed by a number of authors, e.g., Krieg and Krieg [1977], Schreyer, Kulak, and Kramer [1979], Iwan and Yoder [1983], Ortiz and Popov [1985], Ortiz and Simo [1985]. In the

present context, we proceed as follows.

Three points on the yield surface are selected which are representative of wide range of possible states of stress. These points, labeled A, B, and C and shown on Figure 4.1, correspond to uniaxial, biaxial, and pure shear stress, respectively. To construct the isoerror maps we consider for each selected point on the yield surface a sequence of specified normalized strain increments. The stresses corresponding to the (homogeneous) states of strain prescribed in this manner, are then computed by application of the algorithm. At each point the normalization parameters are chosen as the elastic strains associated with initial yielding. Without loss of generality, the calculation is performed in terms of principal values of the strain and stress tensors; i.e., it is assumed that $\epsilon_{12} = 0$. Results are reported in terms of the relative root mean square of the error between the exact and computed solution, which is obtained according to the expression

$$\delta := \frac{\sqrt{(\boldsymbol{\sigma} - \boldsymbol{\sigma}^*) : (\boldsymbol{\sigma} - \boldsymbol{\sigma}^*)}}{\sqrt{\boldsymbol{\sigma}^* : \boldsymbol{\sigma}^*}} \times 100. \tag{4.1}$$

Here, $\boldsymbol{\sigma}$ is the result obtained by application of the algorithm, whereas $\boldsymbol{\sigma}^*$ is the exact solution corresponding to the specified strain increment. The exact solution is obtained utilizing expressions (A.3) through (A.5) in the Appendix. It is noted, however, that for any given strain increment, repeated application of the algorithm with increasing number of subincrements, yields a solution that converges rapidly to the exact solution developed in the Appendix. This provides an additional numerical verification of this solution.

The isoerror maps corresponding to points A, B, and C are shown in Figures 4.2 through 4.4. The values reported here were obtained for a von-Mises yield condition with no hardening and a Poisson ratio of 0.3. It is noted now that Figures 4.3 and 4.4 exhibit a symmetry which may be expected from the location of points B and C on the yield surface. From these results, it may be concluded that the level of error observed is roughly equivalent to that previously reported in the literature for other return mapping algorithms. As a rule, good accuracy (within 5 percent) is obtained for moderate strain increments of the order the characteristic yield strains. It is also noted that exact results for any strain increment are obtained for radial loading along both symmetry axes, as expected.

4.2 Numerical simulations.

The results corresponding to the numerical solution of two boundary value problems are reported below. The main objective of these simulations is to exhibit the reliable performance of the algorithm in practical calculations. The overall robustness of the algorithm is significantly enhanced by combining the classical Newton procedure with a line search algorithm. This strategy has been suggested by number of authors, i.e., see Dennis and Schnabel [1983], or Luenberger [1984]. The specific algorithm used is a linear line search which is invoked whenever a computed energy norm is more than 0.9 of a previous value in the load step (see Matthies and Strang [1979]). Attention also is directed to the excellent convergence characteristics of the Newton procedure. This is the result of the use of the consistent tangent operator developed in Section 2.3. The numerical simulations reported below were performed by implementing the algorithm described in Box 3.1 in an enhanced version of the general purpose nonlinear finite element computer program FEAP described in Chapter 24 of Zienkiewicz [1977].

Example 4.1. *Extension of a strip with a circular hole.* The geometry and finite element mesh for the problem considered are shown in Figure 4.5. A unit thickness is assumed and the calculation is performed by imposing uniform displacement control on the upper boundary. For obvious symmetry considerations only one-quarter of the specimen need be analyzed. A total of 164 4-node isoparametric quadrilaterals with bilinear interpolation of the displacement field are employed in the calculation. It should be noted that for plane stress problems no special treatment of the incompressibility constraint is needed. A von Mises yield condition with linear isotropic hardening is considered. The elastic constants and non-zero parameters in hardening law (3.8) are as follows:

TABLE 4.1. Strip with circular hole. Error norms. $h = 0.01$

Energy Norm			
Load Step			
1	2	3	4
0.112e+01	0.709e-01	0.716e-01	0.725e-01
0.277e-03	0.597e-04	0.248e-03	0.250e-04
0.218e-04	0.100e-04	0.262e-04	0.336e-05
0.504e-06	0.494e-07	0.139e-07	0.944e-06
0.142e-08	0.153e-12	0.245e-10	0.302e-08
0.441e-14	0.396e-22	0.201e-19	0.650e-13
0.690e-25	0.183e-33	0.180e-33	0.334e-22
			0.392e-33
Euclidean norm of residual			
Load Step			
1	2	3	4
0.114e+02	0.285e+01	0.285e+01	0.285e+01
0.388e-01	0.263e-01	0.450e-01	0.230e-01
0.387e-01	0.319e-01	0.439e-01	0.963e-02
0.624e-02	0.165e-02	0.942e-03	0.422e-02
0.215e-03	0.237e-05	0.360e-04	0.279e-03
0.411e-06	0.361e-10	0.135e-08	0.120e-05
0.155e-11	0.175e-15	0.164e-15	0.276e-10
			0.189e-15

TABLE 4.2. Strip with circular hole. Error norms. $h = 0.07$

Energy Norm		**Residual Norm**	
Load Step		Load Step	
1	2	1	2
0.344e+01	0.355e+01	0.199e+02	0.199e+02
0.149e-01	0.139e-02	0.123e+00	0.102e+00
0.997e-01	0.287e-03	0.880e+00	0.612e-01
0.162e-01	0.103e-04	0.718e+00	0.109e-01
0.386e-02	0.300e-07	0.385e+00	0.646e-03
0.716e-05	0.707e-12	0.150e-01	0.317e-05
0.608e-06	0.497e-21	0.407e-02	0.693e-10
0.973e-08		0.547e-03	
0.480e-13		0.163e-05	
0.325e-23		0.147e-10	

$$E = 70, \quad \nu = 0.2, \quad \kappa_0 = 0.243, \quad K = 2.24 \tag{4.2}$$

The problem is first solved using prescribed increments of vertical displacement on the upper boundary of 0.04 followed by three subsequent equal increments of 0.01. The resulting spread of the plastic zone is shown in Figure 4.6. Note that spread of the plastic zone across

an entire cross-section is achieved in the third load increment. The values of the H^1-energy norm and the Euclidean norm of the residual for the entire calculation are shown in Table 4.1. These results clearly exhibit an asymptotic rate of quadratic convergence. It is noted that no line search was required during the iteration process.

TABLE 4.3. Strip with circular hole. Error norms. $h = 0.5$

Energy Norm				**Residual Norm**	
Load Step (line search)				Load Step	
1		2		1	2
0.175e+03	0	0.182e+03	2	0.142e+03	0.142e+03
0.438e+00		0.434e-01		0.546e+00	0.207e+00
0.502e+01	7	0.344e-02		0.133e+01	0.141e+00
0.877e-01		0.182e-03		0.115e+01	0.393e-01
0.207e+01	8	0.172e-05		0.155e+01	0.576e-02
0.244e-01		0.154e-09		0.113e+01	0.433e-04
0.113e-01		0.186e-17		0.732e+00	0.505e-08
0.228e-01	2	0.103e-30		0.545e+00	0.347e-14
0.172e-02				0.284e+00	
0.358e-03				0.176e+00	
0.122e-04				0.196e-01	
0.119e-04	0			0.943e-02	
0.279e-06				0.191e-02	
0.135e-09				0.525e-04	
0.512e-16				0.302e-07	
0.717e-29				0.136e-13	

To demonstrate the robustness of the solution procedure, the problem described above was resolved using two equal increments, $h = 0.07$. The results are reported in Figure 4.7(*a*),(*b*). Figure 4.7(*a*) shows nonconverged solutions, labeled ① and ②, corresponding to the first two iterations of the first load step. Figure 4.7(*b*) shows the converged solution for the two load steps. Note the substantial change in the plastic zone during the iteration process and the complete agreement for the solution previously computed in four steps. The values of the energy and residual norms for the entire iteration process along with the number of line searches performed in each iteration are shown in Table 4.2. A quadratic rate of asymptotic convergence is again exhibited.

Finally, to demonstrate the possible range of application of the proposed procedure the problem was solved now using two increments of $h = 0.5$. Nonconverged solutions corresponding to the first two iterates are shown in Figure 4.8(*a*), while the converged solutions for the two time steps, labeled ① and ②, are shown in Figure 4.8(*b*). These results demonstrate that even with the entire specimen plastified in the first two iterations the solution procedure is still able to produce a converged meaningful solution. The values of the energy and residual norms for the entire iteration process along with the number of line searches performed in each iteration are shown in Table 4.3. For this large loading step a quadratic rate of asymptotic convergence is still exhibited.

Example 4.2. *Bending of a strip with a circular notch* The problem considered is pure bending of a finite width strip with two symmetric circular notches, as shown in Figure 4.9. By noting symmetry and asymmetry conditions, only one quarter of the region need be modeled. The finite element mesh, also shown in Figure 4.9, consists of 252 four node isoparametric elements with bi-linear interpolation functions. Loading is applied by prescribing the boundary condition as a linear varying vertical displacement along the upper boundary.

That is

$$v(x, y, t)\Big|_{y=9} = \frac{x}{b} t, \quad 0 \le x \le b \tag{4.3}$$

where b is a constant given by $b = 10 - 2.5\sqrt{2}$. Four loading increments of equal size, corresponding to $h = 0.1$, are considered. For the geometry described above, two sets of material parameters were analyzed

TABLE 4.4 Strip with circular notch. Error norms.

Isotropic hardening

Energy norm			
Load step			
1	2	3	4
0.403e+01	0.409e+01	0.417e+01	0.296e+01
0.148e-02	0.127e-01	0.228e-02	0.109e-02
0.155e-03	0.658e-02	0.695e-04	0.359e-04
0.178e-06	0.213e-04	0.616e-07	0.429e-07
0.467e-12	0.134e-06	0.415e-09	0.755e-13
0.152e-22	0.647e-12	0.143e-17	0.517e-24
	0.793e-22	0.180e-31	
Euclidean norm of residual			
Load step			
1	2	3	4
0.205e+02	0.205e+02	0.205e+02	0.170e+02
0.977e-01	0.234e+00	0.186e+00	0.112e+00
0.153e+00	0.535e+00	0.729e-01	0.382e-01
0.358e-02	0.557e-01	0.185e-02	0.186e-02
0.614e-05	0.345e-02	0.208e-03	0.273e-05
0.354e-10	0.883e-05	0.131e-07	0.716e-11
	0.967e-10	0.179e-14	

Case (a): Linear isotropic hardening The non-zero material parameters are chosen as

$$E = 100, \quad \nu = 0.3, \quad \kappa_0 = 1.0, \quad K = 5.0 \tag{4.4}$$

The results of the numerical simulation are shown in Figure **4.10**. To provide an idea of the computational effort involved in the calculation, the error in the H^1-energy norm and the Euclidean norm of the residual for each iteration are given in Table **4.4**.

Case (b): Combined linear isotropic-kinematic hardening The non-zero material parameters are chosen as

$$E = 100, \quad \nu = 0.3, \quad \kappa_0 = 1.0, \quad K = 1.0, \quad H = 4.0 \tag{4.5}$$

The results of the numerical simulation are shown in Figure **4.11**, and the corresponding values of the energy and residual norms for each iteration are summarized in Table **4.5**.

The quadratic rate of asymptotic convergence of the Newton iteration scheme is again exhibited by these results. Note that although included in the solution scheme, no line searches are required during the iteration process reported above.

TABLE 4.5 Strip with circular notch. Error norms: Isotropic and kinematic hardening

Energy norm			
Load step			
1	2	3	4
0.403e+01	0.409e+01	0.417e+01	0.296e+01
0.148e-02	0.128e-01	0.214e-02	0.719e-03
0.155e-03	0.659e-02	0.716e-04	0.136e-04
0.178e-06	0.213e-04	0.221e-06	0.110e-07
0.467e-12	0.134e-06	0.388e-09	0.202e-14
0.152e-22	0.642e-12	0.153e-17	0.201e-27
	0.779e-22	0.166e-31	
Euclidean norm of residual			
Load step			
1	2	3	4
0.205e+02	0.205e+02	0.205e+02	0.170e+02
0.977e-01	0.233e+00	0.191e+00	0.120e+00
0.153e+00	0.536e+00	0.761e-01	0.261e-01
0.358e-02	0.557e-01	0.420e-02	0.941e-03
0.614e-05	0.345e-02	0.202e-03	0.449e-06
0.354e-10	0.880e-05	0.133e-07	0.143e-12
	0.958e-10	0.172e-14	

5. Closure.

A consistent return mapping algorithm for plane stress elastoplasticity has been developed. Attention has been directed to the case of von Mises yield condition with nonlinear isotropic and linear kinematic hardening. It has been shown that satisfaction of the consistency reduces to the solution of a *scalar* nonlinear equation. A feature of practical significance is the development of the tangent matrix by consistent linearization of the algorithm. This matrix although different from the classical elastoplastic matrix reduces to it in the limit of infinitesimal loading steps. Use of the consistent tangent matrix ensures a quadratic rate of asymptotic convergence in Newton's method, as demonstrated in the numerical examples discussed above.

The accuracy of the proposed algorithm has been assessed by isoerror maps corresponding strain increments for typical stress states initially on the yield surface. The magnitude of observed errors is comparable to results previously reported for return mapping algorithms associated with plane strain and three dimensional applications.

A closed form solution to the plane stress elastoplastic problem was developed for the customary assumption of constant strain rate over the loading increment. This result, used to construct isoerror maps, may also be employed in explicit transient calculations requiring high accuracy.

The numerical examples presented demonstrate the efficiency and usefulness of the proposed algorithm in practical applications. These examples also exhibit the significant enhancement in the robustness of Newton's method when the proposed algorithm is employed in conjunction with a linear line search.

Acknowledgements: We wish to thank J.W. Ju for his assistance in the computation of the isoerror maps, and to J. Nagtegaal for helpful comments. Partial support for this research was provided by a grant from Lawrence Livermore National Laboratory. This support and the continued interest of Drs. G. L. Goudreau and J. O. Hallquist are gratefully acknowledged.

References

ARGYRIS J.H., J. St. DOLTSINIS, W.C. KNUDSON, L.E. VAZ and K.S. WILLAM, [1979], "Numerical Solution of Transient Nonlinear Problems," *Comp. Meth. Appl. Mech. Engng.*, **17/18**, 341-409.

CHORIN, A., T.J.R. HUGHES, M.F. McCRACKEN, and J.E. MARSDEN, [1978], "Product formulas and numerical algorithms," *Commun. Pure Appl. Math.* **31**, *pp.205-256.*

DENNIS, J.E. and R.B. SCHNABEL. [1983], *Numerical Methods for Unconstrained Optimization,* Prentice-Hall, Inc., Englewood Cliffs, N.J.

HALLQUIST, J.O., [1984], "NIKE2D: A Vectorized, Implicit, Finite Deformation Finite Element Code for Analyzing the Static and Dynamic Response of 2-D solids," *University of California,* Lawrence Livermore National Laboratory, Rep. UCID-19677.

HALLQUIST, J.O., D.J. BENSON and G.L. GOUDREAU, [1985], "Implementation of a Modified Hughes-Liu Shell into a Fully Vectorized Explicit Finite Element Code," (To appear).

HINTON, E. and D.R.J. OWEN, [1980], *Finite Elements in Plasticity: Theory and Practice,* Pineridge Press, Swansea, Wales.

HUGHES, T.J.R. [1983], "Analysis of Transient Algorithms with Particular Emphasis in Stability Behavior," in *Computational Methods for Transient Analysis*, (Edited by T. Belytschko and T.J.R. Hughes). North-Holland Publishing Co.

HUGHES, T.J.R., and TAYLOR, R. L., [1978], "Unconditionally Stable Algorithm for Quasi-Static Elasto/Viscoplastic Finite Element Analysis," *Computer and Structures,* Vol. 8. pp. 169-173.

HUGHES, T.J.R. [1983], "Numerical Implementation of Constitutive Models: Rate-Independent Deviatoric Plasticity," Workshop on *Theoretical Foundations for Large Scale Computations of Nonlinear Material Behavior,* Northwestern University, Evanston, Illinois.

IWAN, D.W., and P.J. YODER [1983], "Computational aspects of strain-space plasticity," *J. Ing. Mech., ASCE,* **109**, pp.231-243.

KRIEG R. D., and S.W. KEY [1976], "Implementation of a Time Dependent Plasticity Theory into Structural Computer Programs," in *Constitutive equations in viscoplasticity: Computational and Engineering aspects, J.A. Stricklin and K.J. Saczalski (eds.), pp.125-137, AMD-20, ASME, New York.*

KRIEG R. D., and D.B. KRIEG [1977], "Accuracies of numerical solution methods for the elastic-perfectly plastic model," *J. Pressure Vessel Tech.*, ASME **99**.

LUENBERGER, D.G., [1984], *Linear and Nonlinear Programming*, Second Edition, Addison-Wesley Publishing Co., Ca.

MARQUES, J.M.M.C., [1984], "Stress Computation is Elastoplasticity," *Engineering Computations,* Vol. 1, Num. 1, 42-51.

MATTHIES, H. and G. STRANG [1979], "The solution of nonlinear finite element equations," *Int. J. Num. Meth. Engng.*, **14**, No. 11, 1613-1626.

MOSS, W.C. [1984], "On the computational significance of the strain space formulation of plasticity theory," *Int. J. Num. Meth. Engng.*, **20**, pp.1703-1709.

NAGTEGAAL, J. C. [1982], "On the implementation of inelastic constitutive equations with special reference to large deformation problems," *Comp. Meth. Appl. Mech. Engng.* **33**.

NAGTEGAAL, J.C., [1985], Private communication.

ORTIZ, M. and E.P. POPOV, [1985], "Accuracy and Stability of Integration Algorithms for Elastoplastic Constitutive Equations," *Int. J. Num. Meth. Engng.* (To appear)

ORTIZ, M. [1981], *Topics in Constitutive Theory for Inelastic Solids*, Ph. D. Dissertation, Dept. of Civil Engineering, University of California, Berkeley.

ORTIZ, M and J.C. SIMO [1984], "An analysis of a new class of algorithms for elastoplastic constitutive relations," *Division of Engineering, Brown University*, Report, Sept. 26, 1984.

SANDLER, I. S. and D. RUBIN, [1979], "An algorithm and a Modular Subroutine for the Cap Model," *J. Geotech. Engng. Div.*, **3**, 173-186.

SCHREYER H. L., R. L. KULAK and J. M. KRAMER [1979], "Accurate numerical solutions for elastic-plastic models," *J. Pressure Vessel Tech.*, ASME **101**.

SIMO J. C., and R. L. TAYLOR, [1985], "Consistent Tangent Operators for Rate Independent Elasto-plasticity," *Comp. Meth. Appl. Mech. Engng.*, **48**, 101-118.

SIMO, J. C. and M. ORTIZ, [1985], "A Unified Approach to Finite Deformation Elastoplasticity Based on the Use of Hyperelastic Constitutive Equations," *Comp. Meth. Appl. Mech. Engng.* (To appear)

SIMO, J.C., [1985], "On the Computational Significance of the Intermediate Configuration in Finite Deformation Elastoplasticity," *Mechanics of Materials* (To appear)

YODER, P.J. and R.L. WHIRLEY [1983], "On the numerical implementation of elastoplastic models," *preprint*

WILKINS, M. L. [1964], "Calculation of elastic-plastic flow," in: B. Alder et al., eds., *Methods of Computational Physics 3* Academic Press, New York.

Appendix: Exact solution for constant strain rate.

The exact solution to the elastoplastic problem of evolution over a typical time step $[t_n\ ,\ t_{n+1}]$ may be obtained under the customary assumption of constant strain rate over the step. For simplicity, reference to kinematic hardening is omitted, so that $\boldsymbol{\alpha} \equiv \mathbf{0}$ and $\boldsymbol{\eta} \equiv \boldsymbol{\sigma}$. By dividing equation (1.13) by λ we obtain the following inhomogeneous linear differential equation

$$\frac{d\boldsymbol{\sigma}}{d\lambda} + \mathbf{D}\mathbf{P}\boldsymbol{\sigma} = \mathbf{D}\frac{d\boldsymbol{\epsilon}}{d\lambda}$$
$$\boldsymbol{\sigma}\Big|_{\lambda=0} = \boldsymbol{\sigma}_n \tag{A.1}$$

subject to the constraint $(1.7)_5$. Equation (A.1) is easily transformed into an integral equation for $\boldsymbol{\sigma}(\lambda)$ of the form

$$\exp[\mathbf{D}\mathbf{P}\lambda]\,\boldsymbol{\sigma}(\lambda) = \boldsymbol{\sigma}_n + \int_{t_n}^{t_{n+1}} \exp[\mathbf{D}\mathbf{P}\tau]\,\mathbf{D}\dot{\boldsymbol{\epsilon}}(\tau)\,d\tau \tag{A.2}$$

Under the assumption that $\dot{\boldsymbol{\epsilon}} = \textit{Constant}$ on $[t_n\ ,\ t_{n+1}]$ one obtains the explicit expression

$$\boldsymbol{\sigma}(\lambda) = \exp[-\mathbf{D}\mathbf{P}\lambda]\,\boldsymbol{\sigma}_n + [\mathbf{D}\mathbf{P}]^{-1}\left[\frac{\mathbf{I} - \exp[-\mathbf{D}\mathbf{P}\lambda]}{\lambda}\right]\mathbf{D}(\boldsymbol{\epsilon}_{n+1} - \boldsymbol{\epsilon}_n) \tag{A.3}$$

As in Section 3, expression (A.3) can be decoupled by introducing the spectral representations of $\mathbf{P}$ and $\mathbf{D}$. On setting $\boldsymbol{\xi}(\lambda) := \mathbf{Q}^t \boldsymbol{\sigma}(\lambda)$, (A.2) reduces to

$$\boldsymbol{\xi}(\lambda) = \exp[-\boldsymbol{\Theta}\lambda]\,\boldsymbol{\xi}_n + \boldsymbol{\Theta}^{-1}\left[\frac{\mathbf{I} - \exp[-\boldsymbol{\Theta}\lambda]}{\lambda}\right]\mathbb{A}_{\mathbf{D}}[\mathbf{Q}^t(\boldsymbol{\epsilon}_{n+1} - \boldsymbol{\epsilon}_n)] \tag{A.4a}$$

where $\boldsymbol{\Theta} := \mathbb{A}_{\mathbf{D}}\mathbb{A}_{\mathbf{P}}$, and

$$\exp[-\boldsymbol{\Theta}\lambda] := diag\{\exp[-\frac{E}{3(1-\nu)}\lambda],\ \exp[-2G\lambda],\ \exp[-2G\lambda]\} \tag{A.4b}$$

One now redefines $\bar{\phi}^2(\lambda)$ in (3.5) by the expression

$$\bar{\phi}^2(\lambda) := \tfrac{1}{2}\boldsymbol{\xi}^t(\lambda)\,\mathbb{A}_{\mathbf{P}}\,\boldsymbol{\xi}(\lambda) \tag{A.5}$$

where $\mathbb{A}_{\mathbf{P}}$ is given by $(1.11c)_2$. As in Section 3, the plastic Lagrange multiplier λ is obtained by solving the consistency condition (3.6). Note that $R(\lambda)$ must be obtained by integrating (1.9). This results in a rather messy expression, except for the trivial case of perfect plasticity.

Remark A.1. It is noted that the basic update formula $(2.8)_2$ follows from the exact expression (A.2) by evaluating the integral over $[t_n, t_{n+1}]$ with the aid of generalized mid-point rule and introducing the the *approximation*

$$\exp[\mathbf{D}\,\mathbf{P}\,\lambda] = \mathbf{I} + \lambda\,\mathbf{D}\,\mathbf{P} + \mathbf{O}(\lambda^2) \qquad \square \tag{A.5}$$

Figure Captions.

Figure 4.1 Plane stress yield surface: Points for isoerror maps.

Figure 4.2 Isoerror map corresponding to point A on yield surface.

Figure 4.3 Isoerror map corresponding to point B on yield surface.

Figure 4.4 Isoerror map corresponding to point C on yield surface.

Figure 4.5 Extension of a strip with a circular hole. Finite element mesh

Figure 4.6 Extension of a strip with a circular hole. Yield zone for the following time increments: ① $h = 0.04$; and ②, ③, and ④ $h = 0.01$.

Figure 4.7 Extension of a strip with a circular hole. (a) Yield zone for first two iterations, labeled ① and ②, corresponding to first time step. (b) Yield zone for converged solutions, labeled ① and ②, respectively. Two time increments of $h = 0.07$.

Figure 4.8 Extension of a strip with a circular hole. (a) Yield zone for first two iterations. The entire specimen is in the plastic regimen. (b) Yield zone corresponding to converged solutions, labeled ① and ②, respectively. Two time increments $h = 0.5$.

Figure 4.9 Bending of a strip with a circular notch. Finite element mesh.

Figure 4.10 Bending of a strip with a circular notch. Case (a) Isotropic hardening ($K = 5.0$). Yield zone for first four loading steps, labeled ①, ②, ③ and ④, respectively. Equal time steps of value $h = 0.1$.

Figure 4.11 Bending of a strip with a circular notch. Case (b) Isotropic and kinematic hardening ($K = 1.0$, $H = 4.0$). Yield zone for first four loading steps, labeled ①, ② ③ and ④, respectively. Equal time steps of value $h = 0.1$.

$E = 30{,}000$ Ksi

$\nu = 0.3$

$\phi = 1/\sqrt{2}\,\|\underset{\sim}{S}\| - R = 0$

$R = \sqrt{3}$

$\sigma_{12} = 0$

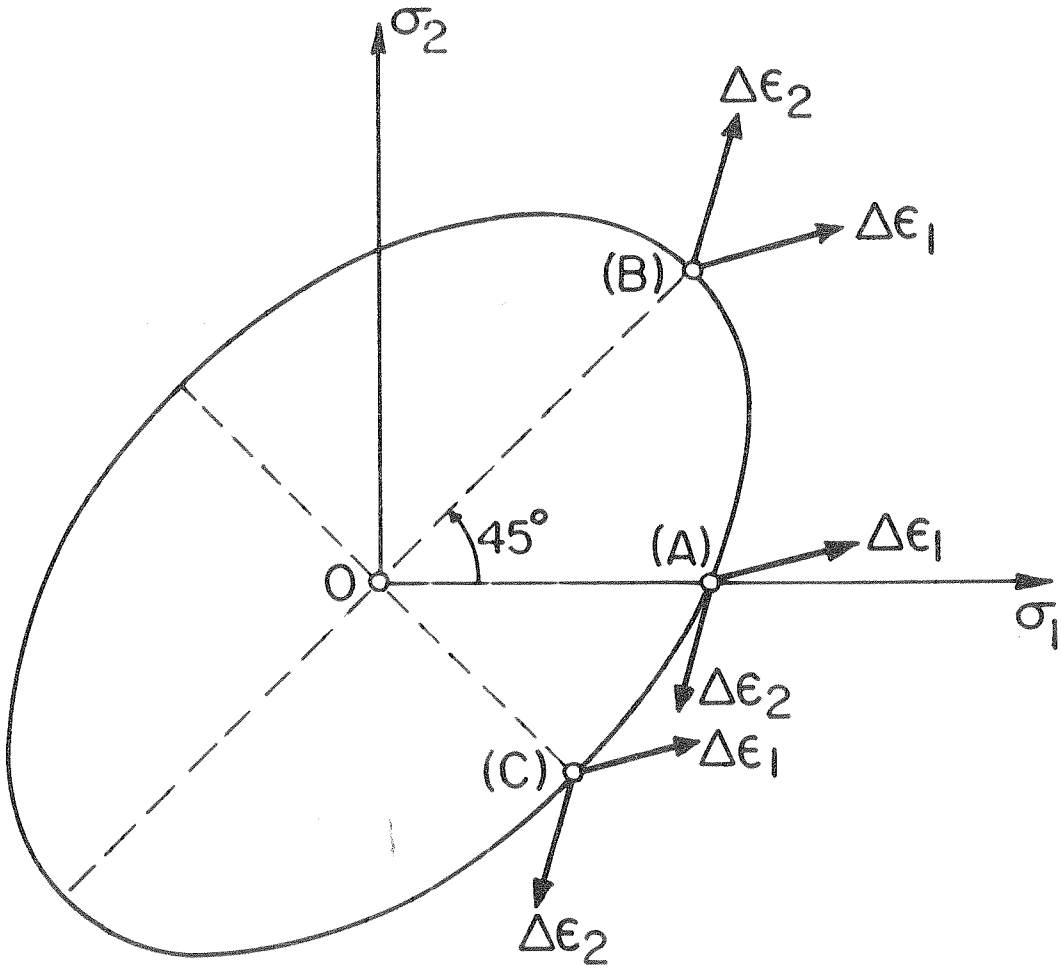

Figure 4.1 Plane stress yield surface: Points for isoerror maps.

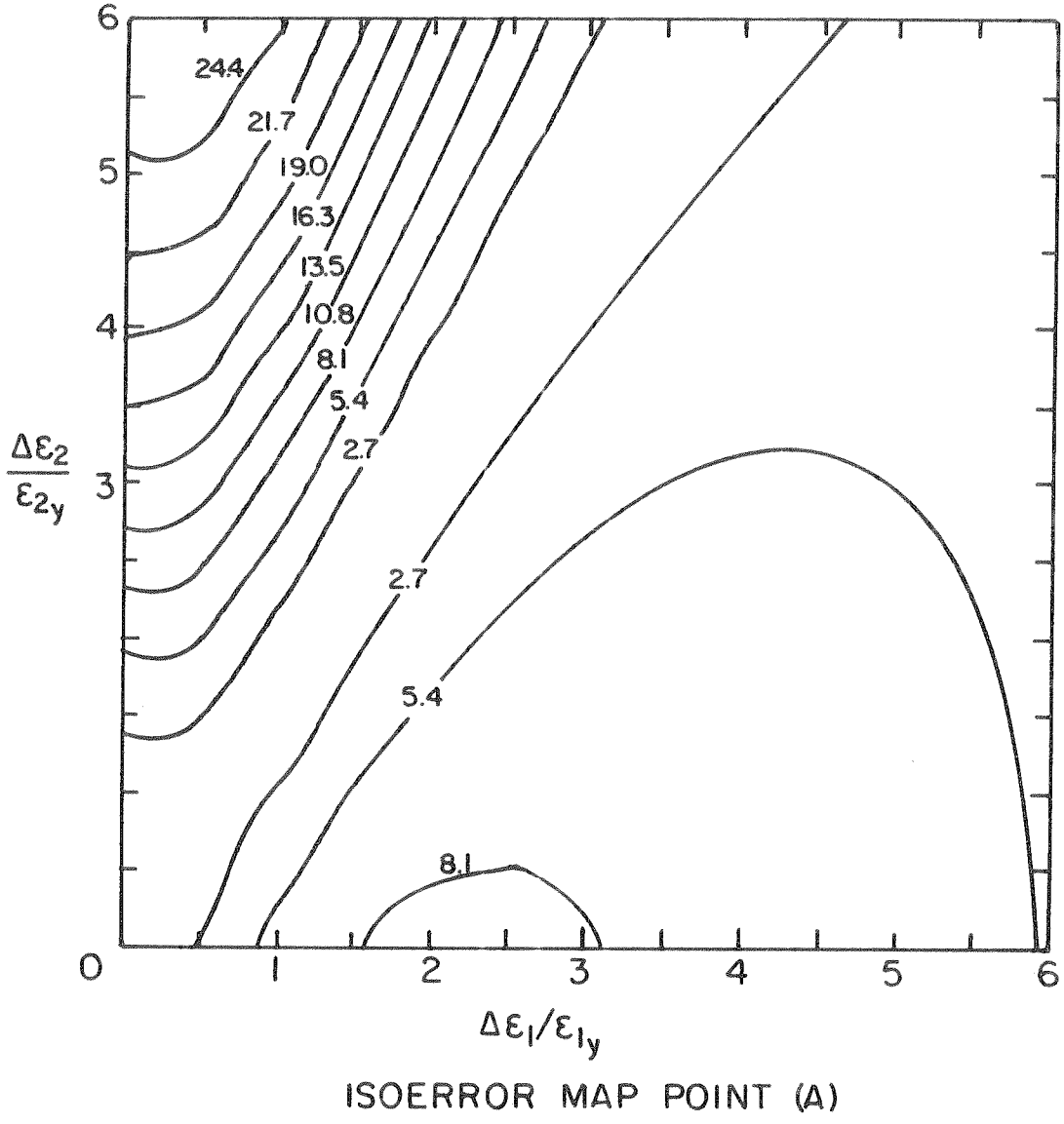

Figure 4.2 Isoerror map corresponding to point A on yield surface.

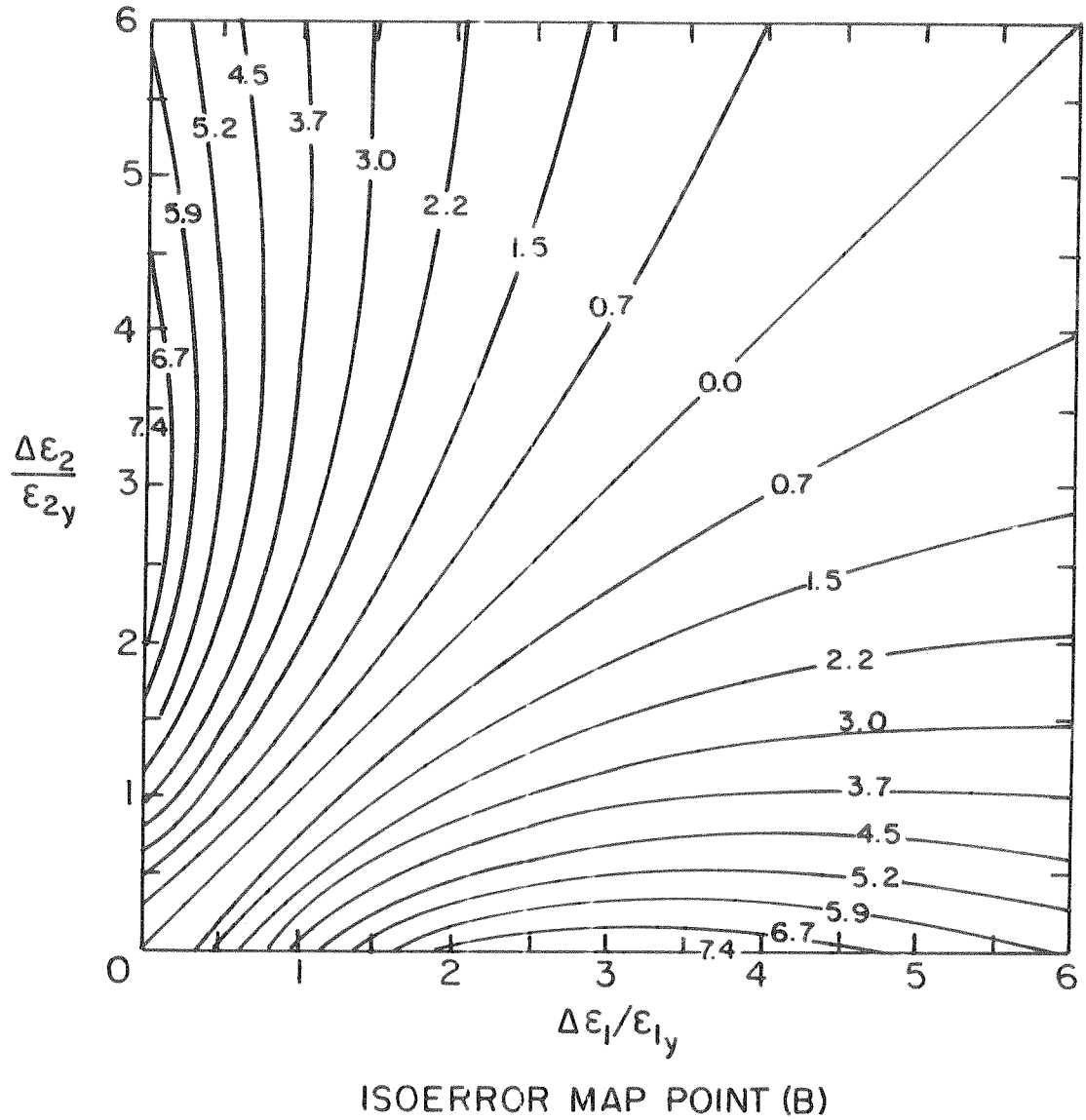

Figure 4.3 Isoerror map corresponding to point B on yield surface.

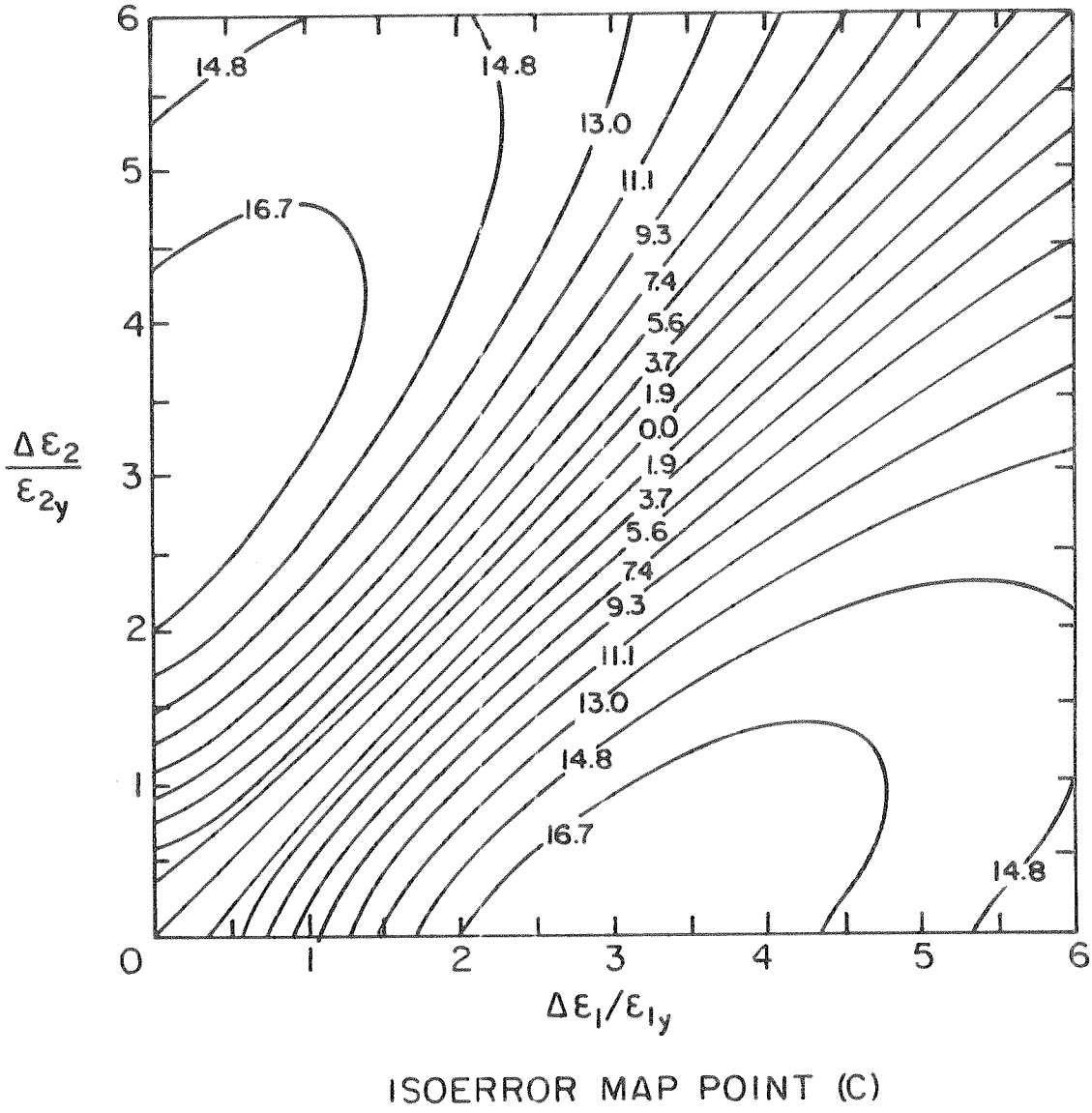

Figure 4.4 Isoerror map corresponding to point C on yield surface.

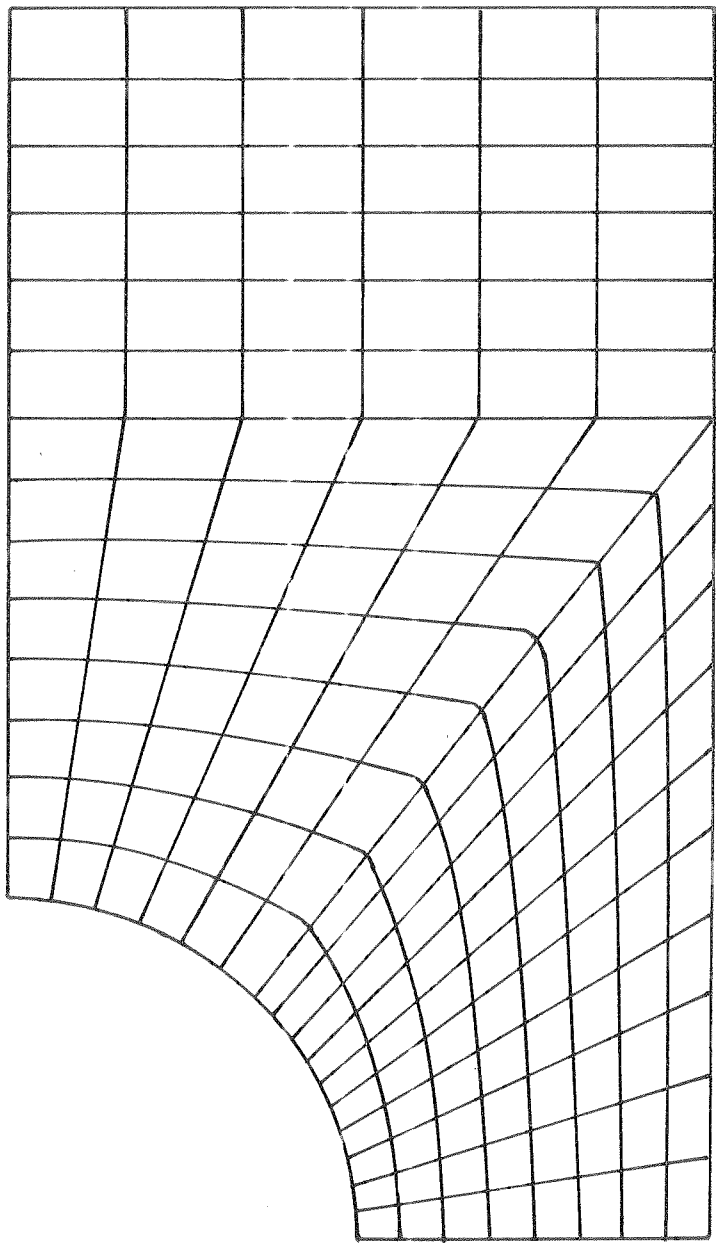

Figure 4.5 Extension of a strip with a circular hole. Finite element mesh

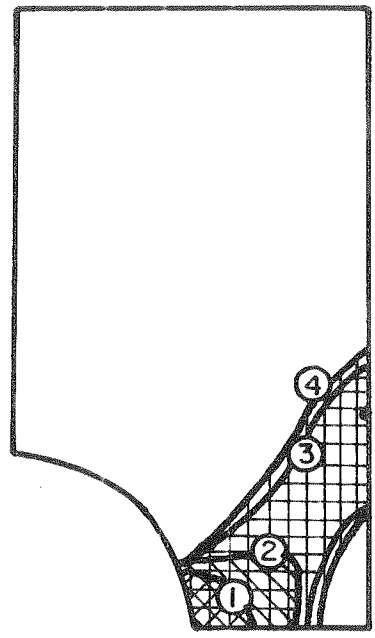

Figure 4.6 Extension of a strip with a circular hole. Yield zone for the following time increments: ① $h = 0.04$; and ②, ③, and ④ $h = 0.01$.

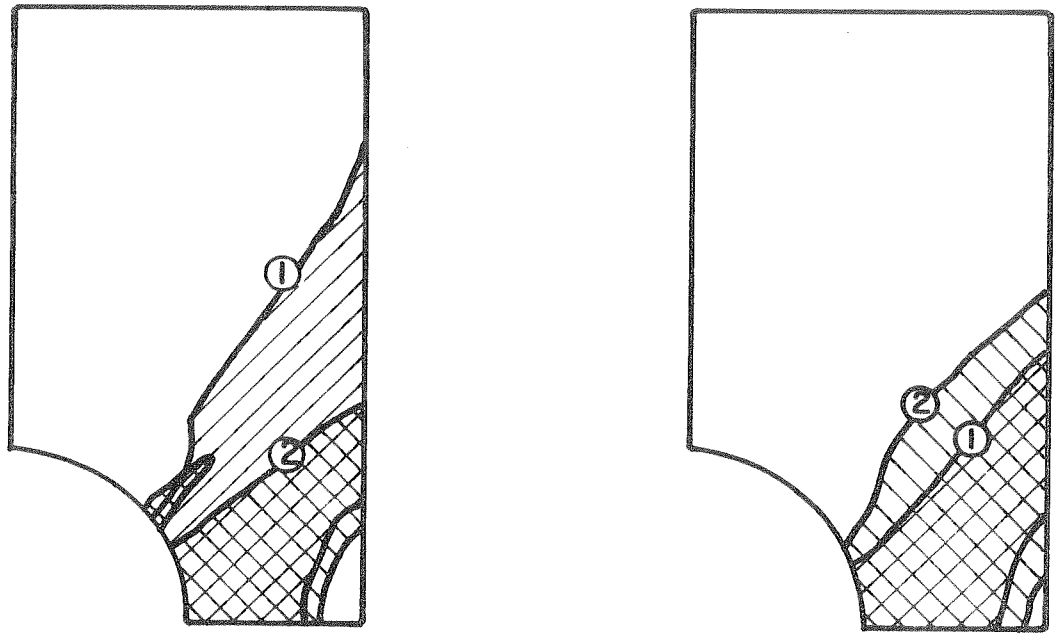

Figure 4.7 Extension of a strip with a circular hole. (a) Yield zone for first two iterations, labeled ① and ②, corresponding to first time step. (b) Yield zone for converged solutions, labeled ① and ②, respectively. Two time increments of $h = 0.07$.

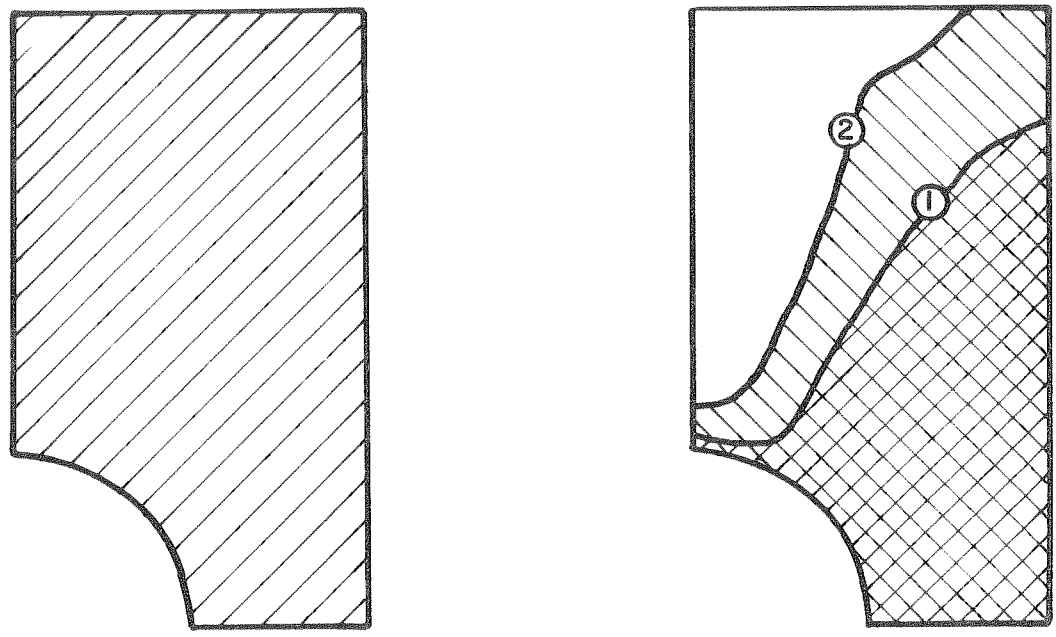

Figure 4.8 Extension of a strip with a circular hole. (a) Yield zone for first two iterations. The entire specimen is in the plastic regimen. (b) Yield zone corresponding to converged solutions, labeled ① and ②, respectively. Two time increments $h = 0.5$.

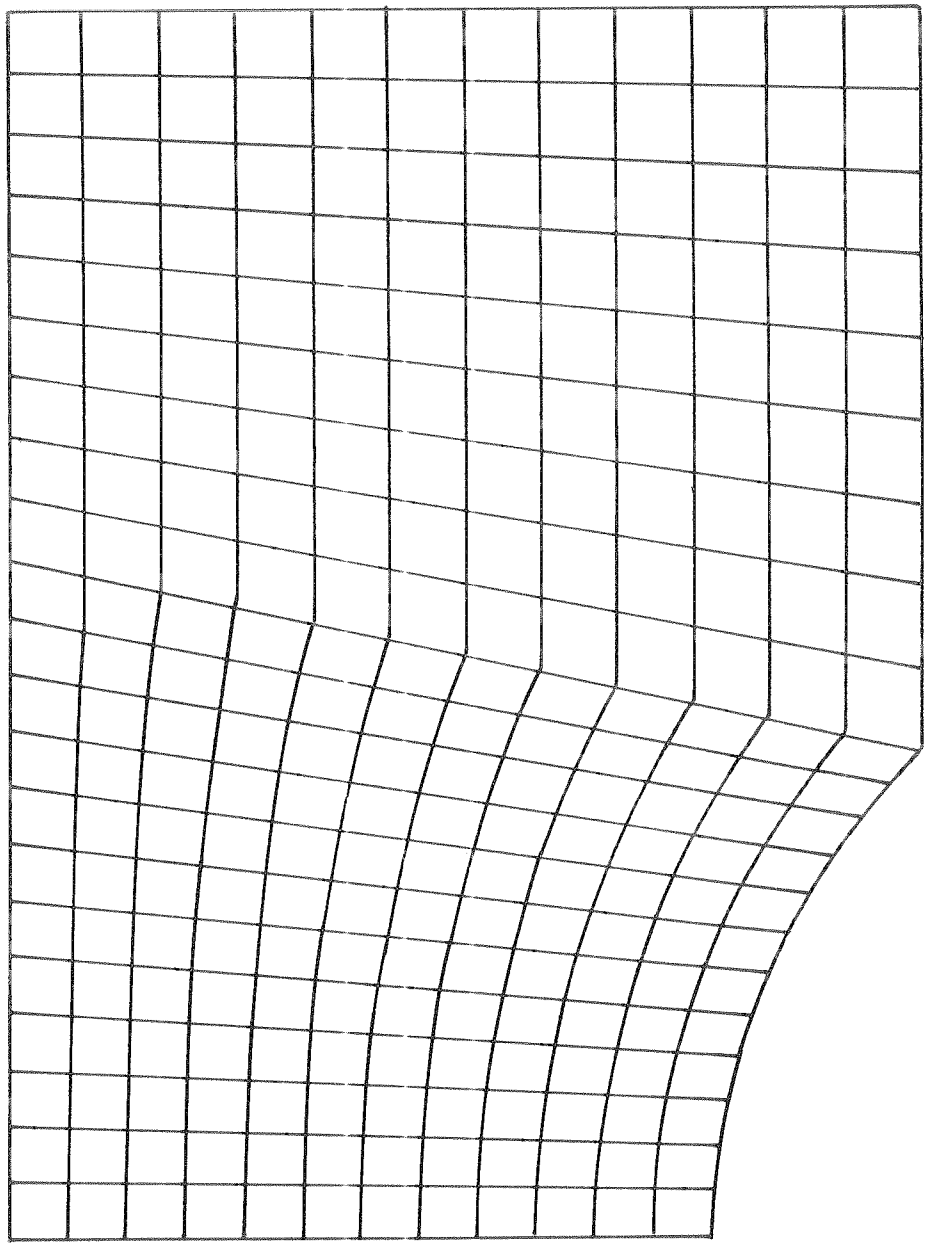

Figure 4.9 Bending of a strip with a circular notch. Finite element mesh.

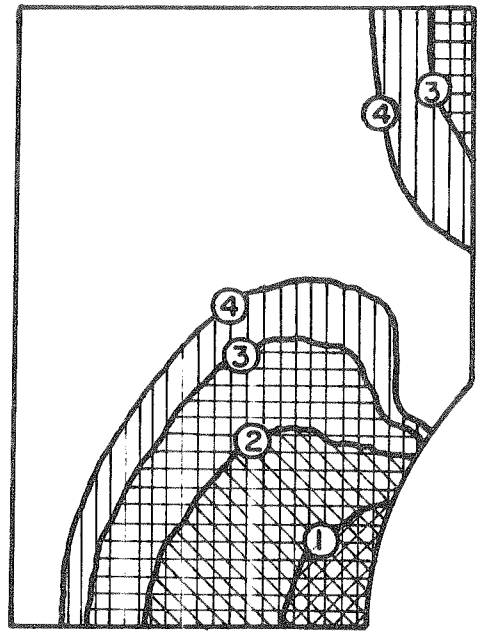

Figure 4.10 Bending of a strip with a circular notch. Case (a) Isotropic hardening ($K = 5.0$). Yield zone for first four loading steps, labeled ①, ②, ③ and ④, respectively. Equal time steps of value $h = 0.1$.

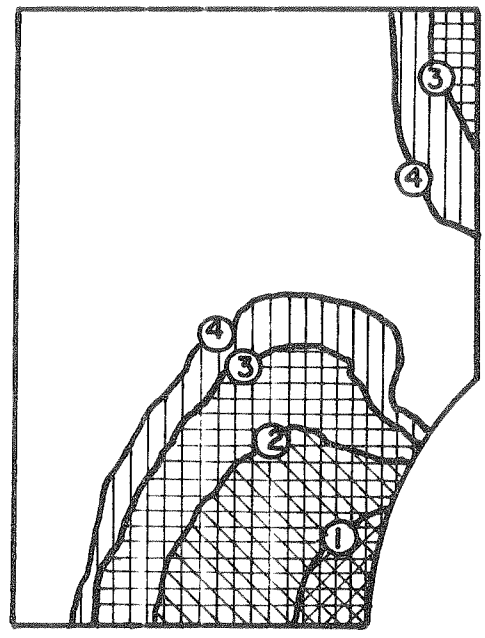

Figure 4.11 Bending of a strip with a circular notch. Case (b) Isotropic and kinematic hardening ($K = 1.0$, $H = 4.0$). Yield zone for first four loading steps, labeled ①, ② ③ and ④, respectively. Equal time steps of value $h = 0.1$.